


Article

Assessment of Agricultural Drought Using Soil Water Deficit Index Based on ERA5-Land Soil Moisture Data in Four Southern Provinces of China

Ruqing Zhang ¹, Lu Li ¹, Ye Zhang ¹, Feini Huang ¹, Jianduo Li ², Wei Liu ³, Taoning Mao ¹, Zili Xiong ¹ and Wei Shangguan ^{1,*} 

- ¹ Southern Marine Science and Engineering Guangdong Laboratory (Zhuhai), Guangdong Province Key Laboratory for Climate Change and Natural Disaster Studies, School of Atmospheric Sciences, Sun Yat-sen University, Guangzhou 510275, China; zhangrq26@mail2.sysu.edu.cn (R.Z.); sysulewlee1@gmail.com (L.L.); Zhangy929@mail2.sysu.edu.cn (Y.Z.); fnhuang.scut@foxmail.com (F.H.); 15113660253@163.com (T.M.); xiongzli@mail2.sysu.edu.cn (Z.X.)
- ² State Key Laboratory of Severe Weather, Chinese Academy of Meteorological Sciences, Beijing 10081, China; jdli@cma.gov.cn
- ³ Guangdong Climate Center, Guangzhou 510275, China; liuwei@gd121.cn
- * Correspondence: shgwei@mail.sysu.edu.cn

Abstract: It is important to accurately assess agricultural drought because of its harmful impacts on the ecosystem and economy. Soil moisture reanalysis datasets provide an important way to assess agricultural drought. In this study, the ERA5-Land surface and subsurface soil moisture was used to estimate the soil water deficit index (SWDI) in four southern provinces of China. The ERA5-Land dataset was evaluated with in situ soil moisture observations from agrometeorological stations. Agricultural drought was assessed for three climate zones at a weekly scale from 2017 to 2019 and was compared with the atmospheric water deficit (AWD). It was found that both ERA5-Land soil moisture and the derived SWDI have relatively high accuracy, and the wet bias in the ERA5-Land dataset can be reduced by the calculation of the SWDI. The subsurface layer has better performance than the surface layer in drought monitoring, though they are highly correlated. Different climate zones demonstrate different drought periods and drought severity, and the temperate climate zone with no dry season has less droughts. The most severe droughts with the largest spatial extent occurred in the early winter, especially in 2019. Differences in the SWDI and AWD are mainly shown in southwestern Yunnan. The results of this study have important reference values for drought risk management.

Keywords: agricultural drought; ERA5-Land; soil moisture; soil water deficit index (SWDI); atmospheric water deficit (AWD)



Citation: Zhang, R.; Li, L.; Zhang, Y.; Huang, F.; Li, J.; Liu, W.; Mao, T.; Xiong, Z.; Shangguan, W. Assessment of Agricultural Drought Using Soil Water Deficit Index Based on ERA5-Land Soil Moisture Data in Four Southern Provinces of China. *Agriculture* **2021**, *11*, 411. <https://doi.org/10.3390/agriculture11050411>

Academic Editor: Brad Ridoutt

Received: 20 March 2021

Accepted: 27 April 2021

Published: 3 May 2021

Publisher's Note: MDPI stays neutral with regard to jurisdictional claims in published maps and institutional affiliations.



Copyright: © 2021 by the authors. Licensee MDPI, Basel, Switzerland. This article is an open access article distributed under the terms and conditions of the Creative Commons Attribution (CC BY) license (<https://creativecommons.org/licenses/by/4.0/>).

1. Introduction

Drought is a frequently occurring natural disaster, which has essential impacts on agriculture, the ecosystem, and the economy [1,2]. Like many parts in the world, China has experienced droughts frequently, and has suffered severe crop yield reductions and other social or economic losses [3,4]. In recent years, the four southern provinces of China (i.e., Yunnan, Guangxi, Guangdong, and Hainan, which cover most of the Pearl River Basin), where about 223 million people reside, suffered from almost annual seasonal droughts due to blocked, low-level monsoons or weakened water vapors. This region has greater high-frequency variability than the other regions in China, which might be owing to the variations in East Asian monsoon precipitation [5]. At the same time, as the global climate warms, there are more droughts in this region, such as the severe drought in Southwest China in 2010 and South China in 2011, which had a disastrous impact on the socio-economic development of these regions [6].

Drought is usually classified into four categories: meteorological drought, agricultural drought, hydrological drought, and socio-economic drought [7]. In this study, the main research object is agricultural drought. Agricultural drought is considered to begin when soil moisture availability reaches such a low level that it cannot provide enough water to crops, and thus negatively affects crop yield. Hence, considering the effects of soil moisture on agricultural production, the availability of soil moisture databases is essential for monitoring and predicting agricultural drought [8]. Generally speaking, the degree of water stress experienced by crops is closely related to the soil moisture content, so soil moisture is usually regarded as an important agricultural drought monitoring indicator [6,9]. Establishing effective and reasonable monitoring indicators to monitor the occurrence, extent, and severity of agricultural drought is very important for agricultural drought monitoring.

The three major sources of soil moisture data are in situ observations, remote sensing, and reanalysis data. Conventionally, soil moisture data are derived from observations of in situ soil moisture networks with different depths and various densities throughout the world [10]. However, the in situ observations have a sparse and uneven distribution, and are even unavailable in some remote regions, which leads to a limited spatial and temporal coverage of soil moisture data [11]. Remote sensing provides good spatial coverage, but is limited to the surface soil layer and may have low accuracy in urban areas and areas with dense vegetation. The development of data assimilation technology enables the production of reanalysis data, which are more representative of observed conditions with less limitations compared to in situ and remote sensing. Reanalysis data have the advantages of global coverage, long time series, no gaps in space and time, and containing subsurface data, which makes them very suitable for the assessment of agricultural drought. Various reanalysis datasets have been developed. Among them, the ERA5-Land soil moisture dataset has relatively high accuracy when it is evaluated and compared to other remote sensing and reanalysis datasets [12], which is why it was chosen in our study.

A variety of indicators have been developed for agricultural drought monitoring [13]. The most widely used agricultural drought indices include the normalized difference vegetation index (NDVI) [14], vegetation condition index (VCI) [15,16], soil water deficit index (SWDI) [17], etc. Since the SWDI has greater biophysical significance than other vegetation indices, climate variables, and even some soil moisture-based methods, it is considered to be a promising method for measuring the available soil moisture for the growth of crops. Many studies have used the SWDI for drought monitoring. Bai et al. evaluated the performance of the SMAP-derived (soil moisture active passive) SWDI for agricultural drought in China [18]. Zhu et al. used the SWDI to assess the agricultural drought situation in the Xiang River Basin, China in 2015–2017 [19]. Martínez-Fernández et al. compared the SWDI with other climate-based drought indices in Spain from 1978 to 2014, and showed very promising results [17].

Many studies have been accomplished to investigate the droughts in the four southern provinces of China. Liu et al. evaluated the droughts of Guangdong from 1956 to 2018 using the standardized precipitation index (SPI) based on rain gauge data [20]. Zhang et al. presented a method for regional frequency analysis based on SPI and assessed the droughts from 1960 to 2005 in the Pearl River Basin based on 42 rain gauging stations [21]. Deng et al. analyzed the spatial and temporal characteristics of rainfall and drought based on the precipitation and temperature data of 48 meteorological stations from 1952 to 2012 in the Pearl River Basin, and showed that the ENSO events have an important influence on seasonal drought in different parts of this region [22]. Li et al. used soil moisture simulation of a land surface model to assess drought in China, and found that the annual monthly drought numbers presented a significant increased trend in the four southern provinces during 1951 to 2008 [23]. Ma et al. used 10-day-scale soil moisture based on remote sensing data to assess agricultural drought in Yunnan province and suggested that the frequency and duration of agricultural drought increased, but the intensity of agricultural drought decreased over the period from 1978 to 2016 [24]. However, previous studies are mostly based on meteorological data and only a few studies are conducted using soil moisture-

based methods in these four southern provinces. In addition, there are no studies that used soil moisture reanalysis data to assess droughts in the four southern provinces, especially in recent years. Therefore, our study intends to use the data from three recent years (from 2017 to 2019) to fill this gap and provide promising methods of dealing with and valuable insights into agricultural droughts.

At present, although there are many studies on the drought situation in the four southern provinces of China, few studies use a soil moisture reanalysis dataset to assess agricultural drought, taking the four southern provinces as a whole. In addition, no studies have used soil moisture site data to evaluate the ERA5-Land data in this area. Moreover, there is no study using the SWDI to reveal the temporal and spatial characteristics of agricultural drought in this region in the past three years. Therefore, this study is aimed at investigating the accuracy of the ERA5-Land soil moisture dataset, its efficiency for drought monitoring, and, thus, the characteristics of agricultural drought in the four southern provinces of China using the ERA5-Land_SWDI. The remaining structure of the paper is organized as follows: the second section introduces the study area, data, methods, and evaluation indices. The third section provides results and discussions. The last section contains the conclusions.

2. Materials and Methods

2.1. Study Area

The four southern provinces include Guangdong, Guangxi, Yunnan, and Hainan. In addition, Hong Kong and Macao are also within the study area, but their areas are small and thus are not mentioned in the following sections. Covering most of the Pearl River Basin, the land of the four southern provinces is mostly in the extent of 18–29° N, 92–117° E. It has a total land area of 846,825 km². As shown in Figure 1, these four southern provinces can be divided into tropical, monsoon climate zone; tropical, savannah climate zone; temperate, no dry season climate zone; temperate, dry winter climate zone; and cold, dry winter climate zone, according to the Köppen climate classification [25]. In this research, we showed the results based on three climate zones: the tropical climate zone (merged by the tropical, monsoon climate zone and the tropical, savannah climate zone); the temperate, no dry season climate zone; and the temperate, dry winter climate zone. The cold, dry winter climate zone in northwestern Yunnan is ignored due to its small area. These four southern provinces are affected by the South Asian and East Asian monsoons, with an average annual precipitation of 1500–2300 mm and a monthly average temperature of 6–25 °C. Although this area has abundant precipitation, the uneven distribution of precipitation has led to frequent droughts and floods. Note that the temperature is almost always above 0 °C, so the growing season is year-round for almost all the places in this study area. This area is populated by about 223 million people and had a gross domestic product of about 2.9 trillion US dollars in 2020.

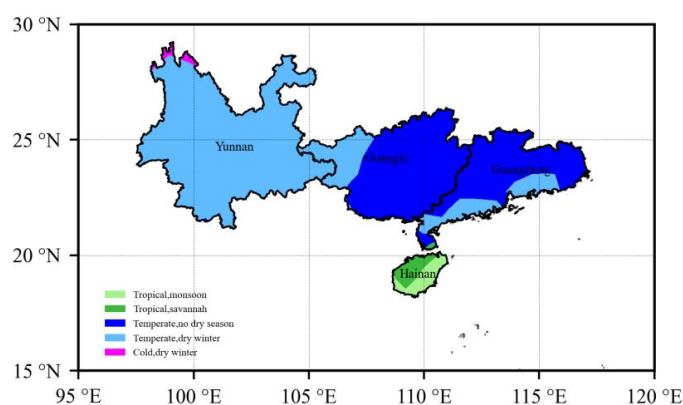


Figure 1. Climate zones according to Köppen–Geiger climate classification in the study area.

2.2. Data

2.2.1. In Situ Data

We used data from 54 meteorological stations from the China Meteorological Information Center, which includes daily precipitation, daily average temperature, and potential evaporation from 2017 to 2019 (Figure 2a).

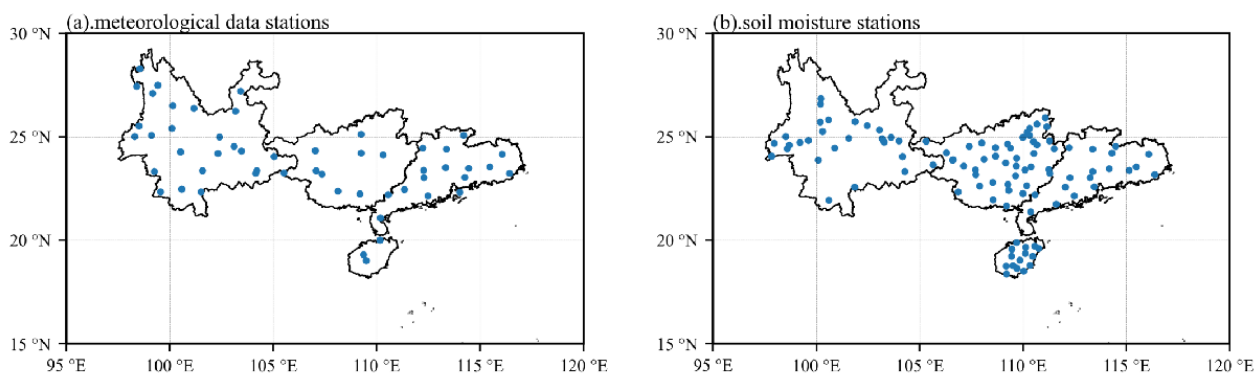


Figure 2. (a) Distribution of meteorological data stations; (b) distribution of soil moisture stations.

The in situ soil moisture data are from agrometeorological stations and were also provided by the CMA. Due to data availability, only the 2017 in situ soil moisture was used in this study. Quality control of the data was carried out as follows: (1) the soil moisture data of the stations at 0, 6, 12, and 18 h were screened from the sites with missing values of less than 10%, and the data of the four time steps were averaged as the daily value; (2) the sites with abnormal conditions (constant values, abnormal spike values, and rising values without precipitation) were eliminated [26,27]. We used the depths of 10 cm and 20 cm as the surface and the subsurface, respectively. In the end, there were a total of 105 sites left with about 38,000 observations for each depth (Figure 2b), which is a large sample size for evaluation.

2.2.2. ERA5-Land Data

The fifth-generation global atmospheric reanalysis data (ERA5) of the European Centre for Medium-Range Weather Forecasts (ECMWF) are the latest generation created by the Copernicus Climate Change Service. In this study, the ERA5-Land, as a part of the ERA5, was chosen, titled “ERA5-Land hourly data from 1981 to present” [28], which includes precipitation, potential evaporation, and soil moisture from 2017 to 2019. The spatial resolution is 0.1° by 0.1°. The first (0–7 cm) and second (7–28 cm) layers of soil moisture were used as the surface and the subsurface, respectively. For the convenience of comparison, both the ERA5-Land and in situ soil moisture were converted into the units of % by volume.

2.3. Methods

The in situ soil moisture data from CMA were used as a reference dataset to evaluate the performance of the surface and subsurface ERA5-Land soil moisture. After the evaluation, the weekly SWDI was calculated to assess the drought condition of the four southern provinces. Additionally, the AWD calculated from meteorological data and the SWDI derived from the ERA5-Land (ERA5-Land_SWDI) were then compared to understand the relationship between the atmospheric drought and the agricultural drought.

2.3.1. Soil Water Deficit Index (SWDI)

The SWDI has shown a good performance in defining drought levels and severity [29]. For example, Zhu et al. used the SWDI calculated from soil moisture activate passive mission to evaluate the agricultural drought in the Xiang River Basin (China), and showed

that the SWDI had a very good agreement with the AWD and can adequately capture the drought dynamics [19]. The surface and subsurface SWDI are calculated as follows:

$$SWDI = \left(\frac{\theta - \theta_{FC}}{\theta_{AWC}} \right) \times 10 \quad (1)$$

$$\theta_{AWC} = \theta_{FC} - \theta_{WP} \quad (2)$$

where θ is the time series of ERA5-Land soil moisture or in situ soil moisture, and θ_{FC} , θ_{WP} , and θ_{AWC} represent the field capacity, wilting point, and available water capacity, respectively. There are several ways to define θ_{FC} and θ_{WP} . In this research, we selected the 5th and 95th soil moisture of the time series to denote θ_{WP} and θ_{FC} [29].

The daily SWDI was computed based on the time series of every grid of the ERA5-Land dataset and every station of the in situ data. Then, the daily SWDI was transferred to a weekly SWDI, and the SWDI was analyzed on a weekly timescale because it is the timescale used in the irrigation schedule [30]. According to Martinez-Fernandez et al. [31], five drought categories are defined according to the SWDI values: no drought (>0), mild ($0 \sim -2$), moderate ($-2 \sim -5$), severe ($-5 \sim -10$), and extreme (< -10). Note that the water deficit is absolute with an SWDI lower than -10 for extreme drought, which means that there is no available water for crops [12].

2.3.2. Percentage of Drought Weeks (PDW)

A drought week is defined when severe or extreme drought occurs with a weekly SWDI value lower than -5 [10]. The percentage of drought weeks (PDW) can represent the drought duration of the four southern provinces. The PDW is calculated as:

$$PDW = \frac{D}{W} \times 100\% \quad (3)$$

where D is the number of drought weeks and W is the total number of study weeks in a year, which was 52 in this study.

2.3.3. Atmospheric Water Deficit Index (AWD)

The AWD is the difference between precipitation and potential evapotranspiration. The AWD is proven to be suitable for reflecting the drought condition related to meteorological parameters [30], and it can also reflect the soil water storage conditions to some extent [17]. The AWD was calculated on a weekly scale:

$$AWD_i = P_i - ET_i \quad (4)$$

where i represents a week of the study period, and P_i and ET_i are the sum of precipitation and the sum of potential evapotranspiration of week i , respectively. The values of these two parameters were taken from the ERA5-Land, both with a unit of mm. AWD values lower than 0 indicate droughts, and AWD values lower than -50 mm indicate extreme droughts.

2.3.4. Evaluation Indices

The Pearson correlation coefficient (R), bias, and root mean square error (RMSE) were calculated to evaluate the applicability and accuracy of the ERA5-Land soil moisture and the performance of the ERA5-Land_SWDI on drought monitoring. The three indices are defined as follows:

$$R = \frac{\sum_{i=1}^n (X_i - \bar{X})(Y_i - \bar{Y})}{\sqrt{\sum_{i=1}^n (X_i - \bar{X})^2} \sqrt{\sum_{i=1}^n (Y_i - \bar{Y})^2}} \quad (5)$$

$$bias = \frac{\sum_{i=1}^n (Y_i - X_i)}{\sum_{i=1}^n X_i} \quad (6)$$

$$RMSE = \sqrt{\frac{\sum_{i=1}^n (Y_i - X_i)^2}{n}} \quad (7)$$

where n is the sample size, X_i and Y_i are the in situ dataset and ERA5-Land dataset, respectively, and \bar{X} and \bar{Y} are the mean value of these two datasets, respectively.

3. Results and Discussion

3.1. Statistical Characteristics of Soil Moisture

Table 1 provides the statistical characteristics of the surface and subsurface soil moisture of the in situ and ERA5-Land data in the three climatic zones in 2017. For the minimum soil moisture, the lowest value appeared in the tropical climate zone for the in situ data, but appeared in the temperate, no dry season climate zone for the ERA5-Land. For the maximum soil moisture, the highest value appeared in the temperate, dry winter climate zone for the in situ data, but appeared in the temperate, no dry season climate zone for the ERA5-Land. Moreover, the ERA5-Land had lower maximum values and higher minimum values than the in situ data. The difference in the minimum and maximum values between the two datasets indicates that the ERA5-Land may have some limitations in representing extreme events. At the same time, the standard deviation of the temperate, no dry season climate zone was much smaller than the other two climate zones, especially for the in situ data, which indicates that the annual variation of soil moisture in the tropical climate zone and the temperate, dry winter climate zone is larger. This is related to the precipitation changes, evapotranspiration, and land surface conditions in these three climate zones. However, the ERA5-Land had larger standard deviations than the in situ data for all climate zone, especially for the temperate, no dry season climate zone, whose standard deviation was 1.5 and 1.8 times that of the in situ data for the surface and subsurface layer, respectively.

Table 1. Statistical characteristics of the surface and subsurface soil moisture (% by volume) of different climate zones.

Layer	Climate	Data	Minimum	Maximum	Mean	Median	Standard Deviation	Number of Observations (grids)
Surface	Tropical	In situ	3.65	59.83	29.25	27.8	5.02	14
		ERA5-Land	13.01	50.95	37.94	38.97	6.01	14
	Temperate, no dry season	In situ	12.27	52.17	30.12	29.90	3.42	42
		ERA5-Land	6.12	51.68	40.48	41.96	5.23	124
	Temperate, dry winter	In situ	6.38	71.02	27.68	26.78	5.31	49
		ERA5-Land	7.49	51.63	38.69	40.70	6.48	193
Subsurface	Tropical	In situ	5.27	57.80	32.01	31.52	4.36	14
		ERA5-Land	14.84	50.65	37.94	38.7	5.75	14
	Temperate, no dry season	In situ	13.9	53.53	32.08	31.55	2.65	42
		ERA5-Land	8.5	51.49	40.66	41.92	4.81	124
	Temperate, dry winter	In situ	7.15	67.62	31.29	31.95	4.55	49
		ERA5-Land	16.32	51.16	39.57	40.68	5.36	193

The range of the surface and subsurface in situ soil moisture average value was about 27–33% in the three climate zones, while the corresponding range of the ERA5-Land was about 37–40%, which is about 9% higher than that of the in situ data. The overestimation of the ERA5-Land will have a certain impact on the later calculation of the SWDI, that is, the surface SWDI will be underestimated. However, this deviation can be eliminated by formulas (1) and (2) to some extent (see Section 3.3), indicating that the surface and subsurface soil moisture values in the ERA5-Land can be properly used for agricultural drought analysis in the four southern provinces. The surface is drier than the subsurface because the surface is more susceptible to external environmental conditions such as solar radiation and surface evaporation, which lead to less water.

3.2. Evaluation of ERA5-Land Soil Moisture and ERA5-Land_SWDI

To verify the accuracy of the ERA5-Land database in the four southern provinces of China, this study used the surface and subsurface in situ soil moisture from the CMA and the corresponding derived weekly SWDI from 1 January 2017 to 31 December 2017 for evaluation.

Generally, the ERA5-Land soil moisture coincides well with the in situ data according to the three evaluation indices (Figure 3). The values of RMSE are mostly between 8% and 20%. The values of R are relatively high (mostly between 0.5 and 0.8), all passing the 99% significance test. Moreover, the average R of the surface and subsurface were 0.68 and 0.73 for the three climate zones, respectively, which are close to the results of Beck et al. [12] and Muñoz-Sabate et al. [28]. Beck et al. evaluated 18 satellite- and model-based soil moisture products based on observations mainly from Europe and the U.S.A. and showed that ERA5-Land is one of the best with an average R of 0.72. Muñoz-Sabate et al. evaluate the ERA5-Land soil moisture using data from over 800 in situ sensors from the International Soil Moisture Network and showed an average R around 0.65. In accordance with the RMSE, the subsurface has a higher R value than the surface for all the climate zones because the surface soil moisture is more affected by meteorological conditions. The bias values are positive (i.e., wet bias) in most cases for all climate zones, and the bias in the subsurface is smaller. Among the three climate zones, the tropical climate zone has a lower average RMSE and bias than the other two, especially for the subsurface. However, the tropical climate zone also has a slightly lower R.

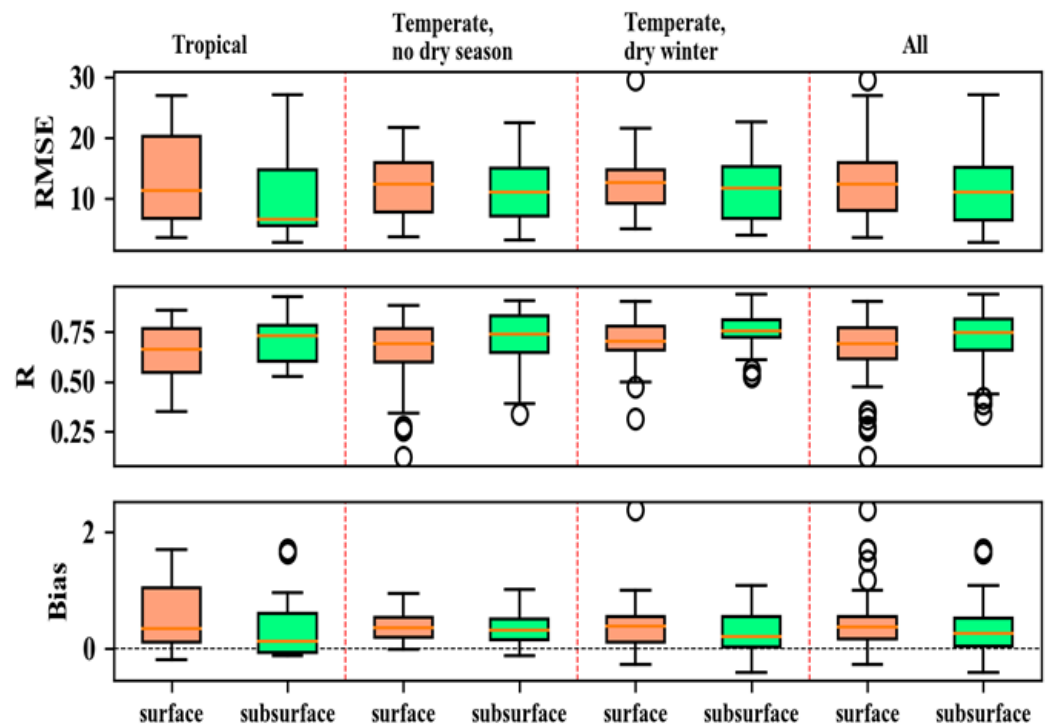


Figure 3. Root mean square error (RMSE), R, and bias of the surface and subsurface soil moisture between the ERA5-Land and in situ data in the three climate zones and the whole study area.

The SWDI calculated by the ERA5-Land dataset was evaluated on a weekly basis (Figure 4). The RMSE values are mostly between 2 and 3.5 in the three climate zones, which are relatively small compared to the range of the SWDI. In addition, the RMSE of the SWDI in the subsurface is much lower than that in the surface, while the RMSE values of soil moisture are quite similar in these two layers. The R values of the SWDI are mostly between 0.4 and 0.8, which are close to those of soil moisture. The bias values are mostly between -0.2 and 0.1 , which are significantly smaller than those of soil moisture. In addition, the median bias of the subsurface is around zero. This may owe to the standardization

in Equation (1) for the calculation of SWDI. Among the three climate zones, generally, the temperate, dry winter climate zone has the best performance according to the three statistics. This is different from the evaluation of soil moisture, which indicates that the performance of the SWDI is not necessarily in accordance with that of soil moisture. Note that it will be valuable to evaluate the uncertainty estimation of ERA5-Land using methods, such as those by Jedlicka et al. [32].

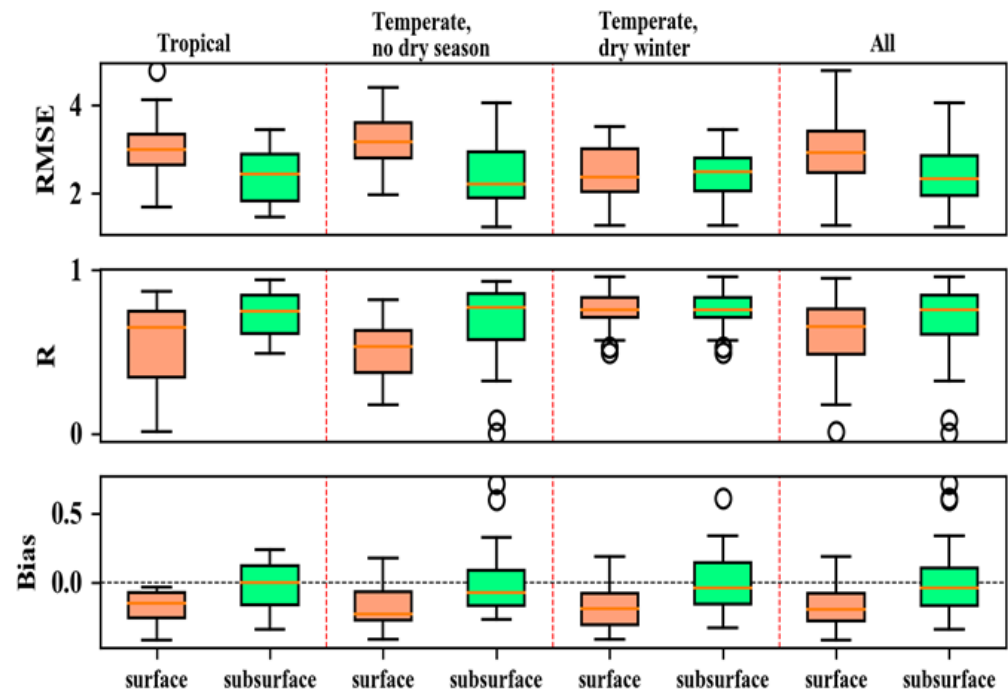


Figure 4. RMSE, R, and bias of the surface and subsurface weekly Soil Water Deficit Index (SWDI) between the ERA5-Land and in situ data in the three climate zones and the whole study area.

The evaluation of soil moisture and the weekly SWDI shows that ERA5-Land has satisfactory performance in the assessment of agricultural drought in the four southern provinces of China. According to the results in Figures 3 and 4, soil moisture and the SWDI of the subsurface can more accurately reflect agricultural drought than those of the surface (lower RMSE, lower bias, and higher R).

3.3. The Relationship between the Surface and Subsurface Weekly ERA5-Land_SWDI

The SWDI in the surface can reflect the changes in agricultural drought affected by meteorological factors, such as precipitation, evaporation, and temperature. For example, Zhu et al. used the surface SWDI index to assess agricultural drought in the Xiang River Basin, China [19]. However, the SWDI in the subsurface can better reflect the effective water storage required for plant growth. For example, Pablos et al. used root zone soil moisture to assess agricultural drought [33]. Therefore, it is necessary to consider both the surface and subsurface for the analysis of agricultural drought. Before analyzing the agricultural drought in the four southern provinces, we firstly analyzed the relationship between the surface and subsurface weekly SWDI by both climate zones and some selected sites.

Figure 5 shows the distribution of the weekly ERA5-Land_SWDI in the surface and subsurface during 2017–2019. The weekly SWDI of the temperate, no dry season climate zone was higher than those of the other two climate zones (mainly above -5), while the values below -5 (i.e., severe and extreme droughts) mainly occurred in the tropical and the temperate, dry winter climate zones, and extreme droughts (< -10) mainly occurred in the subsurface in the temperate, dry winter climate zone. The range of the weekly SWDI in the surface and subsurface were similar, except that the subsurface SWDI had a much larger range than the surface in the temperate, dry winter climate zone. In addition, the

subsurface SWDI was much lower than the surface in the temperate, dry winter climate zone. This is because the 5th soil moisture data of the time series calculated as the θ_{WP} in Equation (2) for the subsurface was relatively larger in the temperate, dry winter climate zone which led to the lower SWDI. Figure 6 shows that the correlation coefficients of the weekly SWDI at the surface and subsurface layers were over 0.9 in most areas, indicating that, overall, the weekly SWDI at the surface and subsurface layers had roughly the same temporal variation.

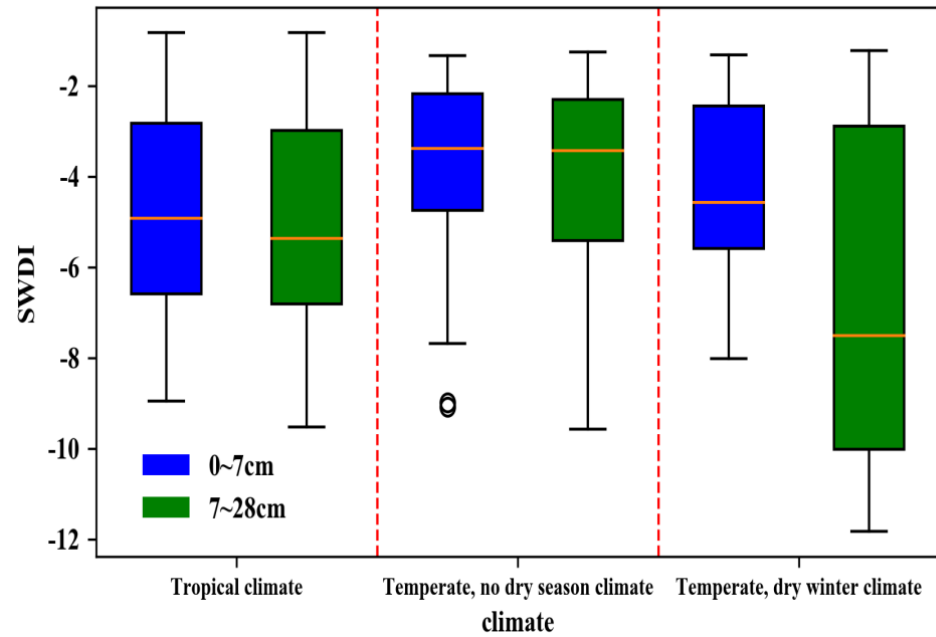


Figure 5. The distribution of the weekly SWDI in the surface and subsurface during 2017–2019.

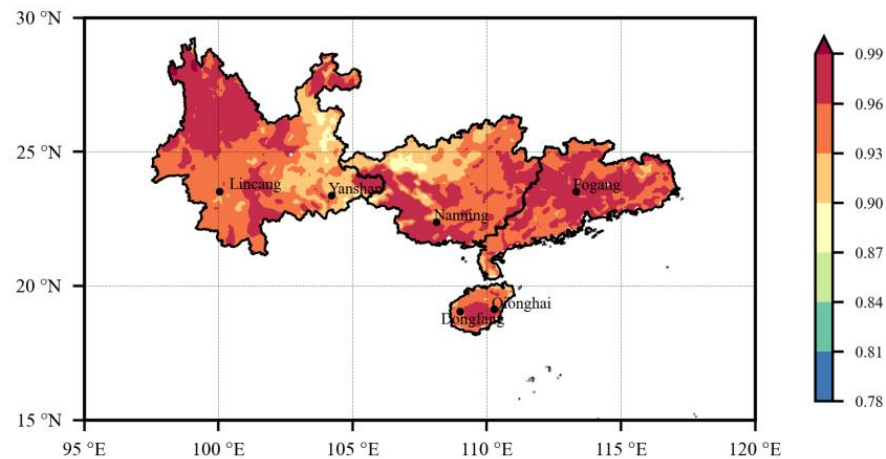


Figure 6. The distribution of Pearson correlation coefficient between the surface and subsurface weekly SWDI during 2017–2019.

According to the distribution of stations in the three climate zones, two stations in each climate zone (Figure 6) were selected to analyze the relationship between the surface and subsurface weekly SWDI indices. It can be seen from Figure 7 that the surface and subsurface weekly SWDI of the 6 sites were very close and had roughly the same trend of variation, though there were more fluctuations in the surface.

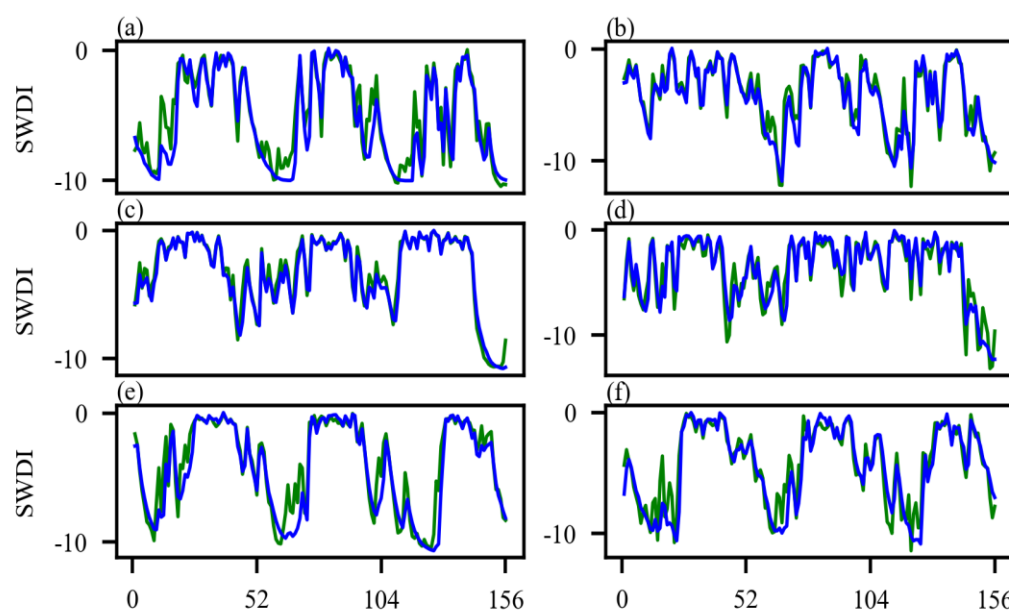


Figure 7. Weekly SWDI index in the surface (solid green line) and subsurface (solid blue line) layers at Dongfang (a), Qionghai (b), Fogang (c), Nanning (d), Lincang (e), and Yanshan (f) sites.

In summary, the surface weekly SWDI was quite close to the subsurface according to the analysis by climate zones and sites. In addition, according to the evaluation in Section 3.2 (Figures 3 and 4), the subsurface SWDI can more accurately reflect the agricultural drought. Moreover, the subsurface stores more water than the surface. Therefore, in the following, the subsurface weekly SWDI was used to analyze the drought conditions in the four southern provinces, which can not only reflect the change of meteorological elements but also show the change of the water storage required for plant growth.

3.4. Drought Estimation in the Four Southern Provinces

In general, our analysis shows similar temporal and spatial characteristics, but with some annual changes from 2017 to 2019. However, our analysis was not intended to reveal the long-term characteristics of agricultural drought, as the three-year period is too short.

3.4.1. Temporal Analysis of the ERA5-Land_SWDI

At the temporal scale, the weekly time series of the ERA5-Land_SWDI from 2017 to 2019 are presented in Figure 8a,c,e for the three climate zones. The weekly time series of the SWDI was mainly between 0 to -10 , and there were only a few very low values (< -10). In general, each climate zone had a similar seasonal trend during the three-year period.

In the tropical climate zone (Figure 8a), the value of the weekly SWDI index ranged from severe to extreme drought (January–April), and then apparently increased to mild and moderate drought (May–September). After September, the drought became moderate and severe (October–December). The variation tendency of the weekly SWDI was mainly related to the concentration of precipitation in this area from May to November, and the higher evapotranspiration increased the drought risk from October to November (Figure 8b). The variation tendency was quite similar in the three years. The most severe drought ($\text{SWDI} < -8$) mainly occurred in March–April (continuous drought) from 2017 to 2019 and December in 2019.

In the temperate, no dry season climate zone (Figure 8c), the weekly SWDI indicated mild and moderate drought (January–September), and then moderate and severe drought (October–December), except for short droughts that happened in the 6th, 14th, and 20th weeks of 2018. The possible reason for this trend may be the high precipitation and low evapotranspiration between January and September and the high evapotranspiration and low precipitation from October to December (Figure 8d). The major difference between the

three years happened between October and December, when the SWDI was much lower in 2019, and a short extreme drought happened in the 44th week of 2017. In addition, the SWDI between March and May was lower in 2018 than in 2017 and 2019.

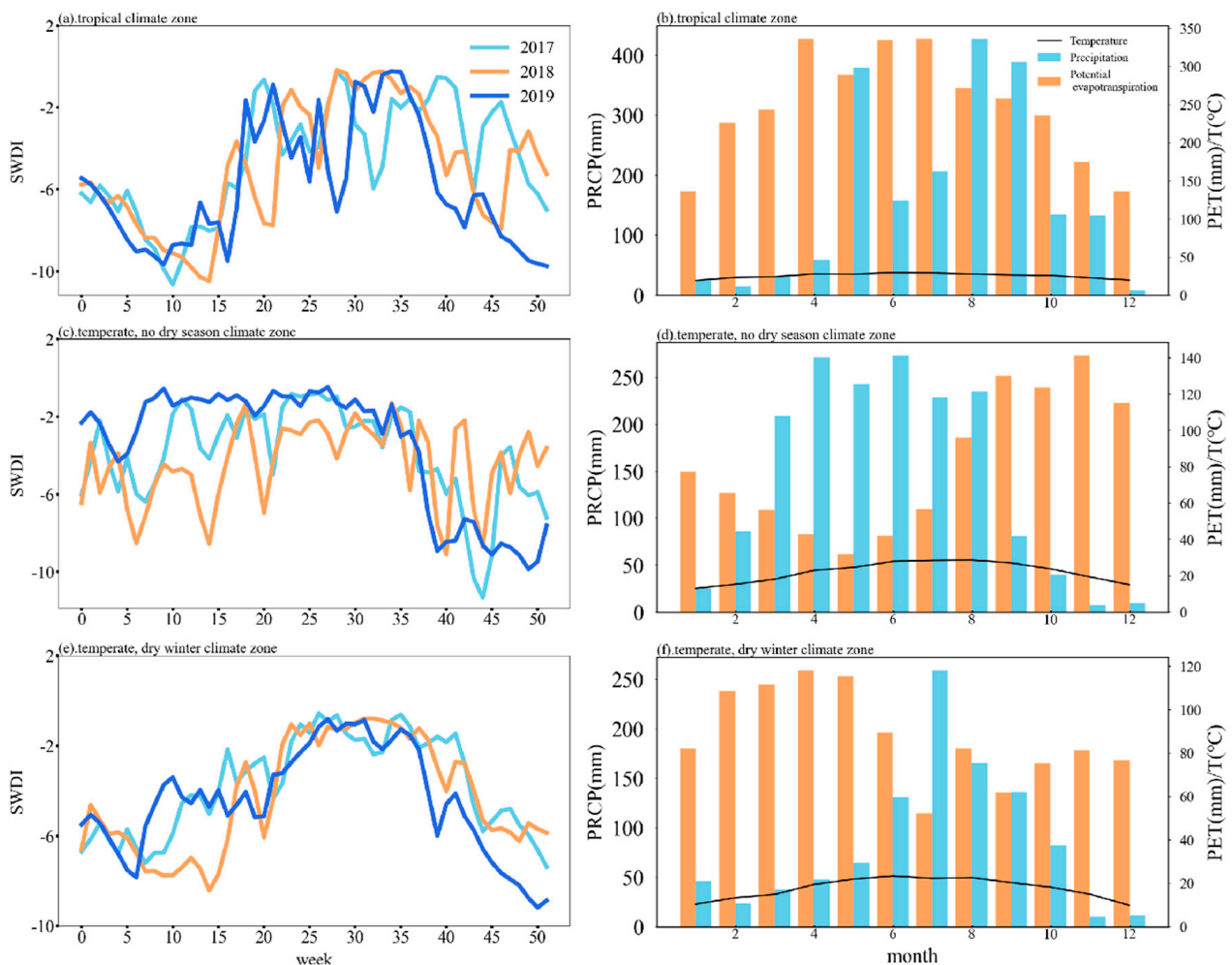


Figure 8. The weekly SWDI (left column) and the monthly temperature (T), precipitation (PRCP), and potential evapotranspiration (PET) (right column) in the tropical climate zone (top row, **a,b**), the temperate, no dry season climate zone (middle row, **c,d**), and the temperate, dry winter climate zone (bottom row, **e,f**) from 2017 to 2019.

In the temperate, dry winter climate zone (Figure 8f), the weekly SWDI ranged from moderate and severe drought (January to May) to mild drought (June to September), and then rapidly decreased to moderate and severe drought (October to December), but there were no extreme droughts. The probable reason for this trend is that precipitation was mainly concentrated between June and September, while other months had higher potential evapotranspiration in this area (Figure 8f). In the three years, the main difference in drought conditions appeared from February to April, when a severe, long-lasting drought happened in 2018. In addition, the SWDI between October and December was lower in 2019 than in 2017 and 2018.

In summary, different climate zones had different drought periods and drought severities, mainly due to their differences in precipitation and evapotranspiration. The temperate, no dry season climate zone had a shorter drought period than the other two climate zones, especially from January to May. The most severe droughts (i.e., the lowest SWDI values) mainly occurred from early winter to the next spring in the tropical climate zone; late autumn and early winter in the temperate, no dry season climate zone; and from winter to the next early spring in the temperate, dry winter climate zone during 2017 to

2019. The three climate zones' changing trends of agricultural droughts, as assessed by the SWDI, are consistent with the analysis of the distribution characteristics of precipitation and drought in the Pearl River Basin by Deng et al. [22]. Their research showed that the drought patterns are not only related to the decreasing trends in rainfall, but also to changes in the daily rainfall concentration, monthly rainfall heterogeneity, and rainfall seasonality. Our results suggest that, in addition to precipitation, agricultural drought is also largely affected by evapotranspiration.

3.4.2. Spatial Analysis of the ERA5-Land_SWDI

The spatial distributions of the SWDI in the 14th, 28th, 40th, and 50th weeks from 2017 to 2019 in this area were selected for comparison (Figure 9). The reasons for this selection are that some typical droughts happened in these weeks (Figure 8), and they are considered to be representative of the droughts in the four seasons, corresponding to middle spring, middle summer, middle autumn, and early winter.

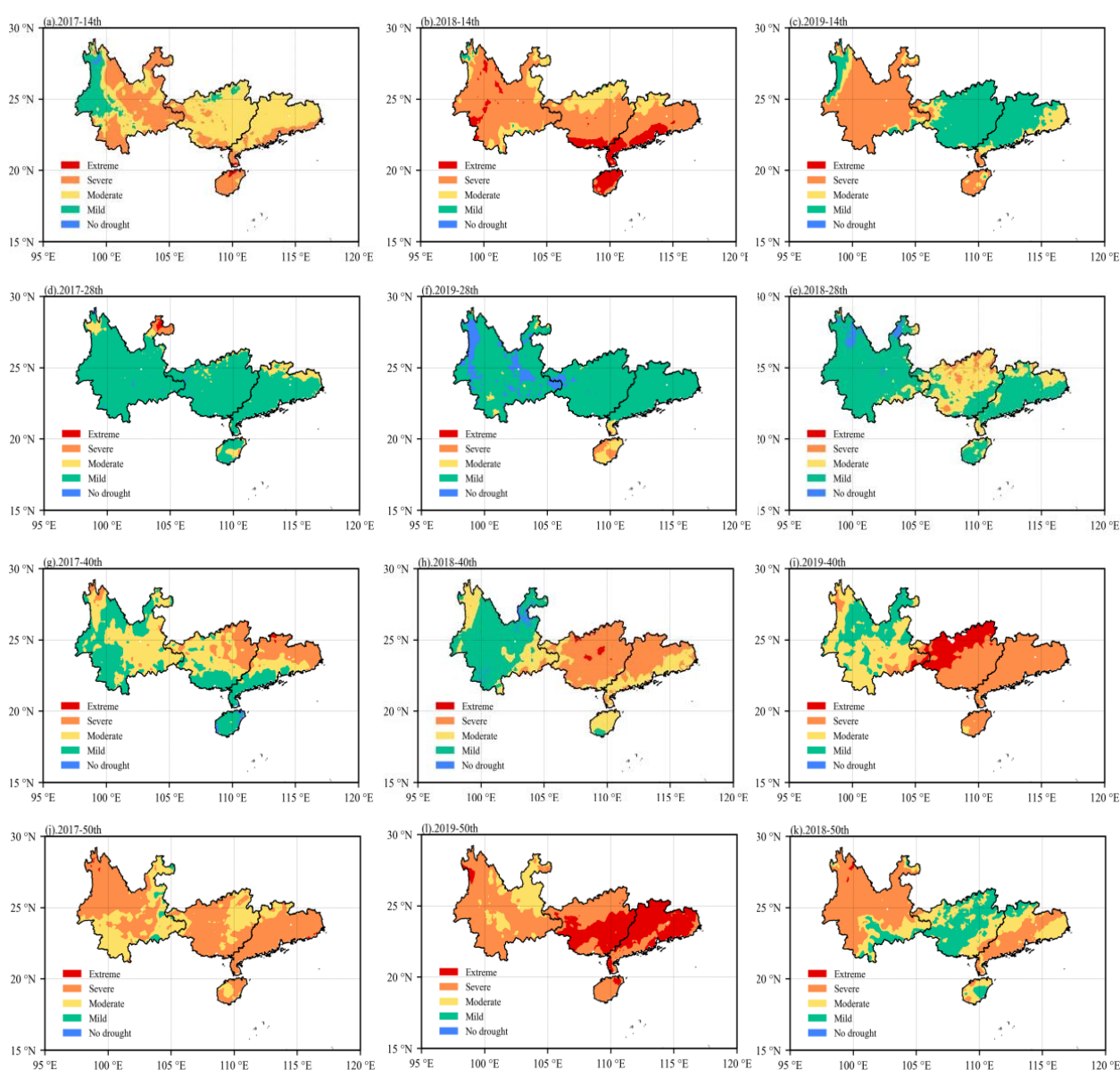


Figure 9. Spatial distribution of the weekly SWDI in the 14th (a–c), 28th (d–f), 40th (g–i), and 50th (j–l) weeks in the four southern provinces of China during 2017–2019.

As shown in Figure 9, in the 14th week, drought in 2018 was apparently more severe than in 2017 and 2019, especially for Hainan and the southern coast of Guangdong and Guangxi. The change on the coast of Guangdong in the temperate, dry winter climate zone was from moderate drought (2017) to extreme drought (2018), and then relieved to a mild drought (2019). Yunnan, also in the temperate, dry winter climate zone, had severe drought in all three years, except for a mild and moderate drought that happened in the western parts in 2017. The overall pattern in the temperate, no dry season climate zone changed from moderate drought (2017), to severe drought (2018), to mild drought (2019). Among them, the southern part of Guangxi experienced extreme drought in 2018. As for the tropical climate zone (Hainan), severe drought happened in 2018 and extreme drought happened in 2017 and 2019.

In the 28th week, most areas had high SWDI values, and there were only mild droughts occurring in most parts of Guangxi in 2018 and Hainan in 2019. This spatial distribution corresponded to the trend of the SWDI in Figure 8a,c,e.

In the 40th week, major droughts happened in Guangxi, Guangdong, and Hainan, with an increasing severity from 2017 to 2019. It is notable that the northwest of Guangxi suffered extreme drought in 2019.

In the 50th week, extreme drought occurred in the temperate, no dry climate zone in 2019, while severe drought occurred in most parts of this climate zone in 2017 and in the east part of this climate zone in 2018. The spatial pattern of droughts was similar among the three years in the temperate, dry winter climate zone, dominated by severe droughts. As for the tropical climate zone, severe droughts happened in most parts of this region in 2017 and 2019, and the drought was not serious in 2018.

In conclusion, from 2017 to 2019, the 50th week witnessed the most severe droughts with the largest spatial extent, while the 28th week had the least droughts. Agricultural droughts in the temperate, no dry season climate zone in the 50th week in 2019 were the most severe with the largest extent. Extreme droughts also happened in Hainan and on the coasts of Guangxi and Guangdong in the 14th week of 2018, and in the northeast of Guangxi in the 40th week of 2019. It can be seen that the agricultural drought severity varies within the same climate zone. The possible reason is that the Köppen climate zones are divided depending mainly on the temperature and precipitation [25]. However, for agricultural drought, in addition to temperature and precipitation, it is also affected by other factors such as surface evapotranspiration, surface vegetation conditions, atmospheric circulation, and topography. For instance, Liu et al. suggested that western Guangdong and the coastal regions, particularly the Pearl River Delta region, have a higher risk of drought [11]. Western Guangdong is dominated by limestone, and serious leakage leading to low soil water storage is caused by the widespread karst caves and underground rivers. In addition, Du et al. also showed that the formation of orographic or convective rain is difficult in western Guangdong because the dominant topographies are plains and terraced terrain, which leads to the stagnation of water [34]. This is another reason for the higher drought risk in western Guangdong.

3.4.3. Temporal Analysis of the PDW

The PDW is divided into four categories: (1) 0–20% (i.e., representing less than 10 weeks of drought events); (2) 20–40%; (3) 40–60%; (4) 60–100% (i.e., representing more than 31 weeks of drought events). A higher percentage of grids that were located in the intervals of 40%–60% and 60%–100% indicated a higher percentage of drought events [10]. The PDW in the four intervals were quantified in the four southern provinces. It can be seen from Figure 10 that the percentages of grids in the four intervals varied among the three years. Most of the PDW values were between 20% and 60%. That is, the number of dry weeks in these three years was about 10–31 weeks. Generally, the PWD values of the subsurface were higher than those of the surface, as there are more values between 40% and 60%, indicating more droughts according to the subsurface. At the same time, the variation tendency of the PDWs was similar for the surface and subsurface in these

three years. Figure 10 shows that the percentage of 20–40% was firstly decreasing, and then rising from 2017 to 2019. However, the percentage of 40–60% showed the opposite trend. Since most of the PDWs were in the interval of 20% to 60%, attention should be paid to drought monitoring in the four southern provinces in the coming years.

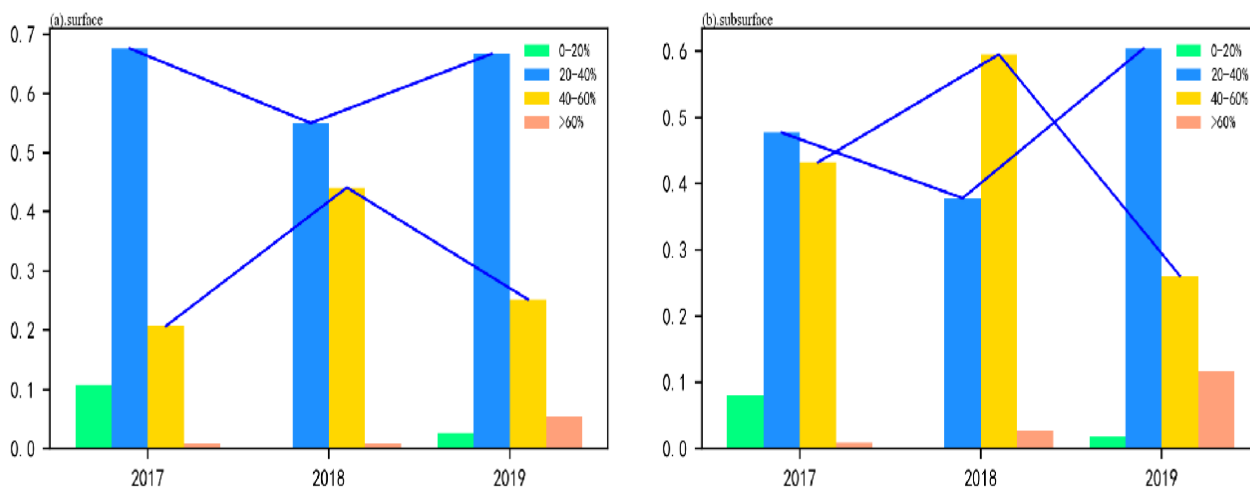


Figure 10. Changes of the Percentage of Drought Weeks (PDW) at the surface (a) and subsurface (b) in four southern provinces of China from 2017 to 2019.

3.4.4. Spatial Analysis of the PDW

Figure 11 illustrates the spatial change in the PDW from 2017 to 2019. Figure 11 illustrates that PDWs followed an increasing trend and then a decreasing trend in the temperate, no dry season climate zone, and the coastal areas in the temperate, dry winter climate zone for both the surface and subsurface. However, western and central Yunnan in the temperate, dry winter and Hainan in the tropical climate zone showed an increasing trend in these three years. In eastern Yunnan and western Guangxi (that is, the upper reaches of the Pearl River Basin), the percentage of dry weeks showed a gradual decrease during these three years. This result is in contrast to the findings of Deng et al. [22], who claimed that the Pearl River Basin's drought conditions have intensified from 1959 to 2012, especially in the Pearl River Basin's upper reaches. However, Wang et al. showed that there were decreasing trends in both drought frequency and duration in the Pearl River Basin's upper reaches from 1950 to 2006 [5]. As our study period is only three years, the long-term trend cannot be identified well, but the decreasing trend in these three years is clear. In general, it can be concluded from the distribution of the PDW that Yunnan in the temperate, dry winter climate zone and Hainan in the tropical climate zone have the highest PDW, followed by the coastal areas in the temperate, dry winter climate zone and the temperate, no dry season climate zone. Among the four provinces, Guangxi had the lowest PDW.

3.5. Comparison between the ERA5-Land_SWDI and the AWD

Meteorological drought is the fundamental cause of agricultural drought, and it is also a prerequisite for agricultural drought. Agricultural drought is the response to the continued meteorological drought in agriculture. There are many meteorological factors causing agricultural drought. Niu et al. found that ENSO or the Indian Ocean dipole had a relationship with the occurrence of extreme hydrological events in the Pearl River Basin [35]. Zhao et al. pointed out that the southern oscillation index and Pacific decadal oscillation were significant factors for precipitation [36]. Fang et al. indicated that sunspot activity had strong relevance in the Pearl River Basin [37,38].

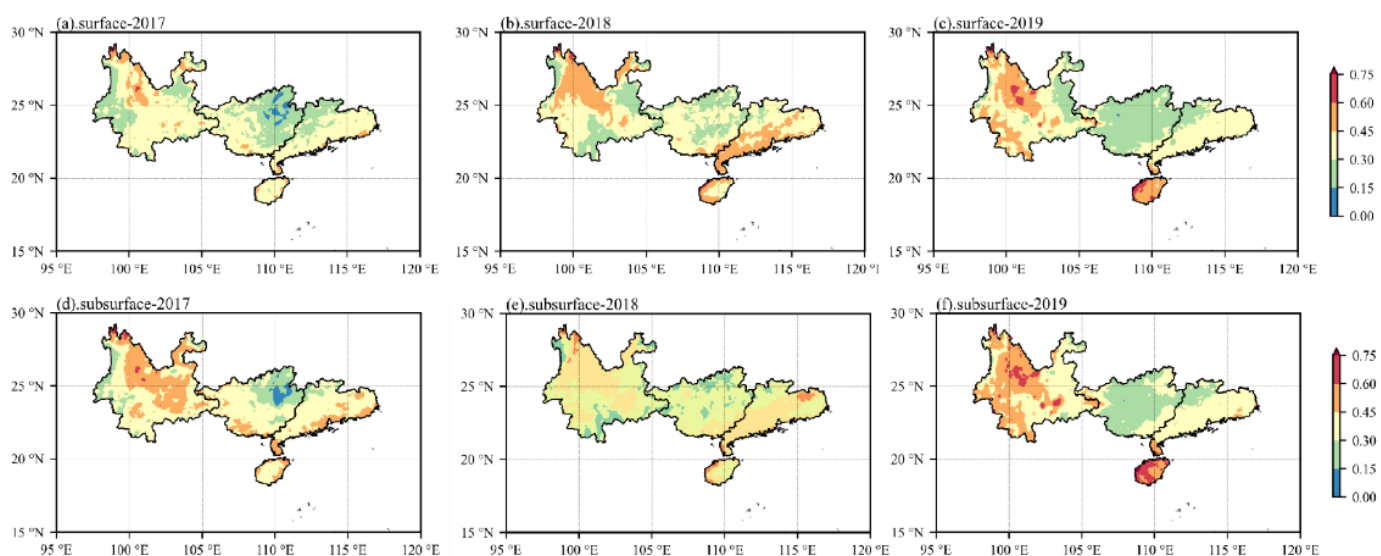


Figure 11. Spatial distribution of the PDW for the surface (a–c) and subsurface (d–f) in the four southern provinces of China during 2017 to 2019.

The purpose of this study was not to find out the meteorological factors that caused agricultural drought from 2017 to 2019, but to explore the relationship between agricultural drought and meteorological drought. The AWD was chosen to analyze this relationship. On the one hand, the AWD widely uses atmospheric data to reflect drought. On the other hand, the AWD can better capture drought dynamics related to the variation of soil water storage [39]. At the same time, changes in soil moisture at the surface and subsurface are closely related to changes in atmospheric moisture. For both the surface or subsurface (Figure 12, not shown for the surface as it is very similar to the subsurface), the correlation coefficients of Guangxi, Guangdong, and Hainan were above 0.25, and the correlation coefficients of Hainan and the coastal areas of Guangdong and Guangxi were above 0.5. The possible reason for the relatively high correlation is that these areas are close to the sea and relatively humid, so precipitation and evapotranspiration are the controlling factors affecting the changes in soil moisture. However, southwestern Yunnan had relatively small correlation coefficients, and some even showed negative correlations. A possible reason is that the surface water in mountainous regions was limited due to the high potential for infiltration because of complex topography [40]. In addition, studies have shown that soil and underlying bedrock, vegetation, and land use may also have important influences on soil moisture dynamics [41]. Thus, the precipitation and evapotranspiration are not the main controlling factors affecting the change in soil moisture, but the land surface conditions [42]. Opposite to this result, Bai et al. [18] showed a high correlation between the AWD and the SWDI based on the remote sensing data (SMAP) in Yunnan. This may be due to the difference in the remote sensing data and the reanalysis data and may need further studies.

In general, the SWDI coincides well with the changes in meteorological conditions, except for areas with more complex topography. The differences between the SWDI and the AWD indicate that agricultural droughts are related not only to meteorological conditions, but also land surface conditions. Thus, it is more proper to use the SWDI to assess agricultural droughts as it directly represents the water storage deficiency.

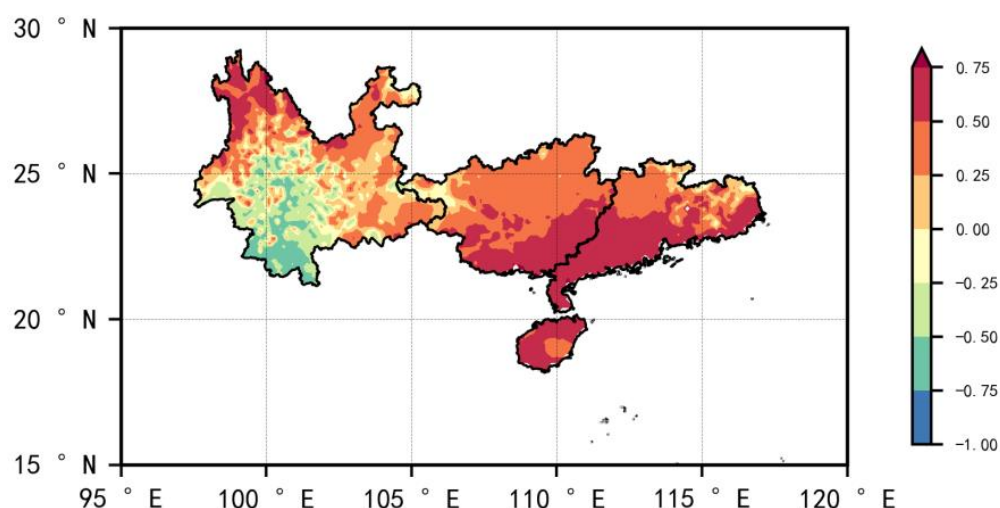


Figure 12. Pearson correlation of the AWD and the SWDI in the subsurface of the four southern provinces of China.

4. Conclusions

In this study, the accuracy of the surface and subsurface soil moisture from the ERA5-Land database was evaluated with in situ soil moisture data from the CMA. In addition, the potential applications of the ERA5-Land database for drought monitoring in the four southern provinces were investigated with a specific agricultural drought index (SWDI). A temporal and spatial analysis was conducted by comparing the ERA5-Land_SWDI and the AWD based on meteorological variables. These two indices were compared from 2017 to 2019. The main conclusions are as follows:

1. There is an overestimation in the ERA5-Land soil moisture compared to the in situ data, but this bias can be reduced by the calculation of the SWDI to some extent, and thus agricultural droughts can be more accurately assessed.
2. Both the ERA5-Land soil moisture and the derived weekly SWDI have relatively high accuracy, and the subsurface layer can more accurately reflect agricultural drought than the surface layer.
3. There is a high correlation between the surface and subsurface ERA5-Land_SWDI.
4. Each of the three climate zones had a similar seasonal trend in the SWDI during 2017–2019. However, different climate zones had different drought periods and drought severities, mainly due to their differences in precipitation and evapotranspiration, and less agricultural droughts happened in the temperate, no dry season climate zone.
5. Among the four selected representative weeks from different seasons, the 50th week (the early winter) witnessed the most severe droughts with the largest spatial extent, while the 28th week (middle summer) had the least droughts. Agricultural droughts in the temperate, no dry season climate zone in the 50th week in 2019 were the most severe with the largest extent. Extreme droughts also happened in Hainan and on the coast of Guangxi and Guangdong in the 14th week of 2018, and in the northeast of Guangxi in the 40th week of 2019.
6. According to the PDW, Yunnan in the temperate, dry winter climate zone and Hainan in the tropical climate zone have a longer drought period than other areas in the four southern provinces of China.
7. Except for southwestern Yunnan, where land surface conditions may be the controlling factors of agricultural drought, the SWDI and the meteorological drought index AWD have a relatively high correlation. However, the SWDI is more suitable for agricultural assessment as it directly reflects the water storage deficiency.

The above promising findings portend that the ERA5-Land_SWDI will be a promising tool for monitoring drought with a high spatial and temporal resolution in the four southern provinces in the future. However, a vast amount of works are needed to achieve this goal. First, the analysis period needs to be extended so that the long-term trends and characteristics of agricultural droughts can be assessed, including frequency, number of events, duration, and severity [43]. Second, the comparison of different soil moisture datasets, including remote sensing data and other reanalysis data, can be performed to address the uncertainty in the drought assessment [44]. Third, other drought indexes such as the standard precipitation index and the crop moisture index may need to be compared to explore more aspects of drought [20]. Fourth, the effect of different methods of estimating the wilting points and field capacity may need further investigation [17]. Last but not least, as land surface conditions have important influences on agricultural drought, factors such as land use, landform, topography, soil properties, and vegetation should be considered [41].

Author Contributions: Conceptualization, W.S.; methodology, R.Z., W.L. and W.S.; validation, J.L., R.Z. and W.S.; formal analysis, W.S. and R.Z.; investigation, W.S. and R.Z.; writing—original draft preparation, R.Z.; writing—review and editing, W.S., Y.Z., F.H., T.M. and Z.X.; visualization, R.Z. and L.L.; supervision, W.S.; project administration, W.S.; funding acquisition, W.S. All authors have read and agreed to the published version of the manuscript.

Funding: This research was funded by the Natural Science Foundation of China under Grant 41975122, U1811464, and 42088101, the National Key R&D Program of China under Grant 2017YFA0604300, Innovation Group Project of Southern Marine Science and Engineering Guangdong Laboratory (Zhuhai) (NO. 311020008), and the Fundamental Research Funds for the Central Universities, Sun Yat-sen University.

Data Availability Statement: The Köppen climate zone classification map is available at <http://koeppen-geiger.vu-wien.ac.at/shifts.htm>. The in situ soil moisture data are available at <http://data.cma.cn/> with certain permissions. The ERA5-Land dataset is available at <https://cds.climate.copernicus.eu/cdsapp#!/dataset/reanalysis-era5-land?tab=form>.

Acknowledgments: The authors thank the anonymous reviewers for providing such valuable comments.

Conflicts of Interest: The authors declare no conflict of interest.

References

1. Tian, Y.; Xu, Y.P.; Wang, G. Agricultural drought prediction using climate indices based on Support Vector Regression in Xiangjiang River basin. *Sci. Total Environ.* **2017**, *622–623*, 710–720. [[CrossRef](#)] [[PubMed](#)]
2. Zhong, R.D.; Chen, X.H.; Lai, C.G.; Wang, Z.L.; Lian, Y.Q.; Yu, H.J.; Wu, X.Q. Drought monitoring utility of satellite-based precipitation products across mainland China. *J. Hydrol.* **2019**, *568*, 343–359. [[CrossRef](#)]
3. Mishra, A.K.; Singh, V.P. A review of drought concepts. *J. Hydrol.* **2010**, *391*, 202–216. [[CrossRef](#)]
4. Huang, S.Z.; Huang, Q.; Chang, J.X.; Leng, G.Y.; Xing, L. The response of agricultural drought to meteorological drought and the influencing factors: A case study in the Wei River Basin, China. *Agric. Water Manag.* **2015**, *159*, 45–54. [[CrossRef](#)]
5. Wang, A.; Lettenmaier, D.P.; Sheffield, J. Soil Moisture Drought in China, 1950–2006. *J. Clim.* **2011**, *24*, 3257–3271. [[CrossRef](#)]
6. Zhang, X.; Tang, Q.; Liu, X.; Leng, G.; Zhe, L. Soil Moisture Drought Monitoring and Forecasting Using Satellite and Climate Model Data over Southwestern China. *J. Hydrometeorol.* **2017**, *18*, 5–23. [[CrossRef](#)]
7. Wilhite, D.A.; Glantz, M.H. Understanding the Drought Phenomenon: The Role of Definitions. *Water Int.* **1985**, *10*, 111–120. [[CrossRef](#)]
8. Paredes-Trejo, F.; Barbosa, H.; Loukas, A. Evaluation of the SMOS-Derived Soil Water Deficit Index as Agricultural Drought Index in Northeast of Brazil. *Water* **2017**, *9*, 377. [[CrossRef](#)]
9. Park, S.; Im, J.; Park, S.; Rhee, J. Drought monitoring using high resolution soil moisture through multi-sensor satellite data fusion over the Korean peninsula. *Agric. For. Meteorol.* **2017**, *237–238*, 257–269. [[CrossRef](#)]
10. Mishra, A.; Vu, T.; Veettil, A.V.; Entekhabi, D. Drought monitoring with soil moisture active passive (SMAP) measurements. *J. Hydrol.* **2017**, *552*, 620–632. [[CrossRef](#)]
11. Liu, D.; Mishra, A.K.; Yu, Z.B. Evaluating uncertainties in multi-layer soil moisture estimation with support vector machines and ensemble Kalman filtering. *J. Hydrol.* **2016**, *538*, 243–255. [[CrossRef](#)]
12. Beck, H.E.; Pan, M.; Miralles, D.G.; Reichle, R.H.; Dorigo, W.A.; Hahn, S.; Karthikeyan, L.; Balsamo, G.; Parinussa, R.M.; van Dijk, A.I.J.M.; et al. Evaluation of 18 satellite- and model-based soil moisture products using in situ measurements from 826 sensors. *Hydrol. Earth Syst. Sci.* **2021**, *25*, 17–40. [[CrossRef](#)]

13. Wang, H.S.; Rogers, J.C.; Munroe, D.K. Commonly Used Drought Indices as Indicators of Soil Moisture in China. *J. Hydrometeorol.* **2015**, *16*, 1397–1408. [[CrossRef](#)]
14. Rouse, J.W., Jr.; Haas, R.H.; Schell, J.A.; Deering, D.W. Monitoring Vegetation Systems in the Great Plains with ERTS. In *Goddard Space Flight Center 3d ERTS-1 Symp*; NASA: Washington, DC, USA, 1974; 1, pp. 309–317.
15. Kogan, F.N. Droughts of the Late 1980s in the United States as Derived from NOAA Polar-Orbiting Satellite Data. *Bull. Am. Meteorol. Soc.* **1995**, *76*, 655–668. [[CrossRef](#)]
16. Kogan, F.N. Application of vegetation index and brightness temperature for drought detection. *Adv. Space Res.* **1995**, *15*, 91–100. [[CrossRef](#)]
17. Martínez-Fernández, J.; González-Zamora, A.; Sánchez, N.; Gumuzzio, A.; Herrero-Jiménez, C.M. Satellite soil moisture for agricultural drought monitoring: Assessment of the SMOS derived Soil Water Deficit Index. *Remote Sens. Environ.* **2016**, *177*, 277–286. [[CrossRef](#)]
18. Bai, J.Y.; Cui, Q.; Chen, D.Q.; Yu, H.W.; Mao, X.D.; Meng, L.K.; Cai, Y. Assessment of the SMAP-Derived Soil Water Deficit Index (SWDI-SMAP) as an Agricultural Drought Index in China. *Remote Sens.* **2018**, *10*, 1302. [[CrossRef](#)]
19. Zhu, Q.; Luo, Y.L.; Xu, Y.P.; Tian, Y.; Yang, T.T. Satellite Soil Moisture for Agricultural Drought Monitoring: Assessment of SMAP-Derived Soil Water Deficit Index in Xiang River Basin, China. *Remote Sens.* **2019**, *11*, 362. [[CrossRef](#)]
20. Liu, C.L.; Zhang, Q.; Singh, V.P.; Cui, Y. Copula-based evaluations of drought variations in Guangdong, South China. *Nat. Hazards* **2011**, *59*, 1533–1546. [[CrossRef](#)]
21. Zhang, Q.; Xiao, M.Z.; Singh, V.P.; Li, J.F. Regionalization and spatial changing properties of droughts across the pearl river basin. *J. Hydrol.* **2012**, *472–473*, 355–366. [[CrossRef](#)]
22. Deng, S.L.; Chen, T.; Yang, N.; Qu, I.A.; Li, M.C.; Chen, D. Spatial and temporal distribution of rainfall and drought characteristics across the Pearl River basin. *Sci. Total Environ.* **2018**, *619–620*, 28–41. [[CrossRef](#)]
23. Li, M.X.; Ma, Z.G. Soil moisture drought detection and multi-temporal variability across China. *Sci. China Earth Sci.* **2018**, *58*, 1798–1813. [[CrossRef](#)]
24. Ma, S.Y.; Zhang, S.Q.; Wang, N.L.; Huang, C.; Wang, X. Prolonged duration and increased severity of agricultural droughts during 1978 to 2016 detected by ESA CCI SM in the humid Yunnan Province, Southwest China. *CATENA* **2011**, *198*, 105036–105049. [[CrossRef](#)]
25. Franz, R.; Markus, K. Observed and projected climate shifts 1901–2100 depicted by world maps of the Köppen-Geiger climate classification. *Meteorol. Z.* **2010**, *19*, 135–141.
26. Li, C. Towards Automatic Monitoring Approach of Agro-Meteorology for Maize and Wheat (in Chinese). Ph.D. Thesis, Institute of Atmospheric Physics, Chinese Academy of Science, Beijing, China, 2017.
27. Dorigo, W.A.; Xaver, A.; Vreugdenhil, M.; Gruber, A.; Hegyiova, A.; Sanchis-Dufau, A.D.; Zamojski, D.; Cordes, C.; Wagner, W.; Drusch, M. Global automated quality control of in situ soil moisture data from the International Soil Moisture Network. *Vadose Zone J.* **2013**, *12*, 1–21. [[CrossRef](#)]
28. Muñoz-Sabater, J.; Dutra, E.; Agustí-Panareda, A.; Albergel, C.; Arduini, G.; Balsamo, G.; Boussetta, S.; Choulga, M.; Harrigan, S.; Hersbach, H.; et al. ERA5-Land: A state-of-the-art global reanalysis dataset for land applications. *Earth Syst. Sci.* data discuss.
29. Miriam, P.; Martínez-Fernández, J.; Nilda, S.; Angel, G.Z. Temporal and Spatial Comparison of Agricultural Drought Indices from Moderate Resolution Satellite Soil Moisture Data over Northwest Spain. *Remote Sens.* **2017**, *9*, 1168.
30. Torres, G.M.; Lollato, R.P.; Ochsner, T.E. Comparison of Drought Probability Assessments Based on Atmospheric Water Deficit and Soil Water Deficit. *Agron. J.* **2013**, *105*, 428–436. [[CrossRef](#)]
31. Martínez-Fernández, J.; González-Zamora, A.; Sánchez, N.; Gumuzzio, A. A soil water based index as a suitable agricultural drought indicator. *J. Hydrol.* **2015**, *522*, 265–273. [[CrossRef](#)]
32. Jedlicka, K.; Vales, J.; Hajek, P.; Kepka, M.; Pitonak, M. Calculation of Agro-Climatic Factors from Global Climatic Data. *Appl. Sci.* **2021**, *11*, 1245. [[CrossRef](#)]
33. Pablos, M.; González-Zamora, A.; Sánchez, N.; Martínez-Fernández, J. Assessment of SMADI and SWDI agricultural drought indices using remotely sensed root zone soil moisture. *Int. Assoc. Hydrol. Sci.* **2018**, *380*, 55–66. [[CrossRef](#)]
34. Du, Y.D.; Liu, J.L.; Song, L.L. Characteristics and forming causes of drought and its controlling measures in Leizhou peninsula. *Agric. Res.* **2004**, *01*, 28–31.
35. Niu, J. Precipitation in the Pearl River basin, South China: Scaling, regional patterns, and influence of large-scale climate anomalies. *Stoch Environ. Res. Risk Assess.* **2013**, *27*, 1253–1268. [[CrossRef](#)]
36. Zhao, Y.F.; Zou, X.Q.; Cao, L.G.; Xu, X.W.H. Changes in precipitation extremes over the Pearl River Basin, southern China, during 1960–2012. *Quat. Int.* **2014**, *333*, 26–39. [[CrossRef](#)]
37. Fang, W.; Huang, S.Z.; Huang, G.H.; Huang, Q.; Wang, H.; Wang, L.; Zhang, Y.; Li, P.; Ma, L. Copulas-based risk analysis for inter-seasonal combinations of wet and dry conditions under a changing climate. *Int. J. Climatol.* **2019**, *39*, 2005–2021. [[CrossRef](#)]
38. Fang, W.; Huang, S.Z.; Huang, Q.; Huang, G.; Wang, H.; Leng, G.; Wang, L.; Guo, Y. Probabilistic assessment of remote sensing-based terrestrial vegetation vulnerability to drought stress of the Loess Plateau in China. *Remote Sens. Environ.* **2019**, *232*, 111290. [[CrossRef](#)]
39. Liu, W.J.; Liu, C.Q.; Zhao, Z.Q.; Xu, Z.F.; Liang, C.S.; Li, L.B.; Feng, J.Y. Elemental and strontium isotopic geochemistry of the soil profiles developed on limestone and sandstone in karstic terrain on Yunnan-Guizhou Plateau, China: Implications for chemical weathering and parent materials. *J. Asian Earth Sci.* **2013**, *67–68*, 138–152. [[CrossRef](#)]

40. Wang, J.X.; Zou, B.P.; Liu, Y.; Tang, Y.; Zhang, X.; Yang, P. Erosion-creep-collapse mechanism of underground soil loss for the karst rocky desertification in Chenqi village, Puding county, Guizhou, China. *Environ. Earth Sci.* **2014**, *72*, 2751–2764. [[CrossRef](#)]
41. Chen, H.; Zhang, W.; Wang, K.; Fu, W. Soil moisture dynamics under different land uses on karst hillslope in northwest Guangxi, China. *Environ. Earth Sci.* **2010**, *61*, 1105–1111. [[CrossRef](#)]
42. Zhang, D.D.; Yan, D.H.; Lu, Y.F.; Wang, Y.C.; Feng, J. Copula-based risk assessment of drought in Yunnan province, China. *Nat. Hazards* **2015**, *75*, 2199–2220. [[CrossRef](#)]
43. Wang, A.; Kong, X. Regional climate model simulation of soil moisture and its application in drought reconstruction across China from 1911 to 2010. *Int. J. Climatol.* **2021**, *41* (Suppl. S1), E1028–E1044. [[CrossRef](#)]
44. Liu, Y.W.; Liu, Y.B.; Wang, W. Inter-comparison of satellite-retrieved and Global Land Data Assimilation System-simulated soil moisture datasets for global drought analysis. *Remote Sens. Environ.* **2019**, *220*, 1–18. [[CrossRef](#)]